RSC Advances

PAPER

View Article Online
View Journal | View Issue

Cite this: *RSC Adv.*, 2023, **13**, 13592

Using deep eutectic solvent dissolved low-value cotton linter based efficient magnetic adsorbents for heavy metal removal

Sihong Ye,†[a] Mingli Xu,†[b] Hui Sun,[a] Ying Ni,[a] Rui Wang,[a] Runping Ye, *[c] Lingzhong Wan,[a] Fangzhi Liu,[a] Xiaonan Deng*[a] and Juan Wu*[a]

In this study, a novel magnetic bio-adsorbent was synthesized by modifying cotton linter (CL) cellulose with deep eutectic solvents (DESs) and Fe_3O_4 magnetic nanoparticles. The adsorption capacity of CL, Fe_3O_4/CL, Fe_3O_4/CL-oxidation, and Fe_3O_4/CL-DES for Cu^{2+} was 11.0, 66.1, 85.7, and 93.1 mg g^{-1}, respectively, under the optimal adsorption conditions of an initial pH value of 6.0, stirring rate of 300 rpm, and a temperature of 30 °C. The presence of Fe_3O_4 nanoparticles increased the proportion of hydroxyl groups and thus improved the ion-exchange ability of Cu^{2+}. The dissolution of DES significantly decreased fiber crystallinity and increased the number of hydroxyl group (amorphous regions increased), thus improving the chelation reaction of Cu^{2+}, which was favorable for surface adsorption. In addition, we used the Langmuir and Freundlich isothermal models to simulate the adsorption behavior of Fe_3O_4/CL-DES, and the results indicated that Cu^{2+} follows a Freundlich isotherm model of multilayer adsorption. The fitting of the adsorption kinetics model indicated that the adsorption process involves multiple adsorption mechanisms and can be described by a quasi-second-order model. These results provide a potential method for the preparation of high-efficiency adsorbents from low-value cotton linter, which has broad application prospects in wastewater treatment.

Received 24th February 2023
Accepted 18th April 2023

DOI: 10.1039/d3ra01248d

rsc.li/rsc-advances

1 Introduction

In recent years, heavy metal pollution in soil, sediment, and water environments has garnered worldwide attention due to the high toxicity and ability of heavy metals to accumulate in living organisms.[1–4] Water pollution, in particular, poses a significant threat to ecosystems and human health through the food chain.[5,6] As a result, the safe, cost-effective, and efficient treatment of toxic metal ions in wastewater is a critical area of research. Various physical, chemical, and biological methods are currently employed to remove heavy metals from water, including adsorption, chemical precipitation, electrocatalysis, membranes, and bioremediation.[7–9] Among these, adsorption and photocatalysis are widely used for the removal of different pollutants in wastewater.[10] Adsorption relies on the physical or chemical binding of pollutants to a solid surface, which can be highly effective for certain types of pollutants but may require frequent replacement or regeneration of the adsorbent material.[11] On the other hand, photocatalysis involves the use of catalysts and light energy to initiate chemical reactions that decompose pollutants, which can be effective for a wider range of pollutants but may require more complex and expensive setups.[12] Therefore, adsorption is typically used to remove heavy metals or organic pollutants from industrial wastewater, while photocatalysis may be more suitable for removing emerging pollutants such as pharmaceuticals or personal care products.[13]

Various adsorbent materials have been developed for removing heavy metals from wastewater, including inorganic substances like clay and metal oxides, organic polymers like cellulose and chitosan, carbon-based materials such as activated carbon and graphene, and porous skeleton materials such as MOFs and COFs.[14–18] Biomass-based adsorbents incorporating a cellulose matrix have attracted attention due to their lower cost and improved mass transfer performance.[19–21] Cotton linter (CL) is a staple fiber that remains on the surface of cotton seed after the process of ginning.[22] It can be separated by a lint stripping machine, and the resulting product can be equivalent to 15% ~20% of the total lint.[23] In the 1980s, cotton seeds were typically directly used for oil pressing after refined cotton ginning due to outdated technology, leading to a significant waste of CL. However, with advancements in science and technology, numerous high-value applications for CL have been identified, such as its use as a raw material for the production of

[a]*Institute of Cotton, Anhui Academy of Agricultural Sciences, Hefei, China. E-mail: xn_deng@foxmail.com; ecjtutmtm@163.com*

[b]*Department of Life Sciences, Anhui Agricultural University, Hefei, China*

[c]*Key Laboratory of Jiangxi Province for Environment and Energy Catalysis, Institute of Applied Chemistry, School of Chemistry and Chemical Engineering, Nanchang University, Nanchang, China. E-mail: rye@ncu.edu.cn*

† These authors contributed equally to this work.

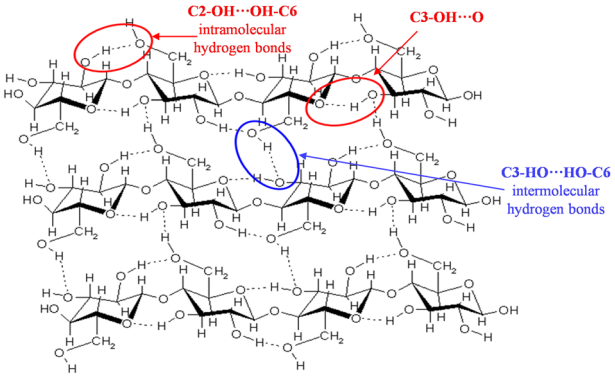

Fig. 1 Macromolecular structure of cellulose.

high-grade paper and the industrial extraction of cellulose.[24–26] Cellulose, which is the main component of CL (Fig. 1), is characterized by a large number of hydroxyl groups, intramolecular and intermolecular hydrogen bonds, and multi-level cavities.[27–29] These structural features make CL suitable for use as an adsorbent through surface adsorption and hydrogen bonding. However, the high crystallinity of cellulose can affect the accessibility of the hydroxyl groups, limiting the ability of contaminant molecules to penetrate the crystalline region of cellulose for reaction and leading to a low adsorption rate of pristine CL.[30,31] Therefore, decreasing the crystallinity of cellulose and increasing the accessibility of the hydroxyl groups are key challenges for improving the adsorption rate of CL.

Ball milling is an effective method to decrease the crystallinity of cellulose and increase its amorphous content. Ling *et al.* used vibratory ball milling to break cellulose crystals, leading to a decrease in molecular weight, an increase in carbonyl groups, and a higher surface area.[32] In contrast to the physical method of ball milling, cellulose can also be dissolved chemically. However, traditional solvents like CS_2 and NMMO have limitations due to high pollution, energy consumption, and instability.[33–35] A new green ionic liquid solvent called 1-butyl-3-methylimidazolide was discovered, but it is expensive and has high viscosity.[36–38] To overcome this, a new type of ionic liquid analogue called deep eutectic solvents (DESs) has emerged, which are low-cost, easy to prepare, non-toxic, and biodegradable.[39–41] Using DESs to dissolve cellulose can increase its reactive form and facilitate subsequent modifications.

Fe_3O_4, a magnetic material, has been widely utilized for the removal of heavy metal pollution from water due to its high affinity towards inorganic metal salt species (such as Cu^{2+}, Pb^{2+}, and Hg^{2+}), resulting in selective adsorption.[42,43] However, most bare Fe_3O_4 materials exhibit low Cu^{2+} adsorption capacities, and the adsorption process is slow, leading to reduced effectiveness and applicability. Against this backdrop, this study investigates the use of Fe_3O_4-loaded treated CL in Cu^{2+} adsorption, and extensively characterizes the structural properties of the adsorbents. Furthermore, the study focuses on the impact of different treatment methods on the crystallinity and hydroxyl group content of CL, and evaluates the adsorption properties in Cu^{2+} removal from aqueous solution under diverse experimental conditions, including the pH and temperature, reusability, and simulation of the adsorption isotherm and kinetic model.

2 Experimental section

2.1 Adsorbent synthesis

Commercially available reagents and solvents were used without further purification. Cotton linter (CL) was obtained from a pure natural experimental base. $Cu(NO_3)_2$, $FeCl_3$, $FeSO_4 \cdot 7H_2O$, $NaIO_4$, NaOH, oxalic acid dihydrate ($C_2H_2O_4 \cdot 2H_2O$), choline chloride, glycerol, and ethanol (C_2H_5OH) were employed as chemical reagents. To compare the efficacy of two modification methods for CL, Fe_3O_4 weight loading was fixed at approximately 20 wt%. The samples obtained through oxidation and deep eutectic solvent modification methods were denoted as Fe_3O_4/CL-O and Fe_3O_4/CL-D, respectively. A typical Fe_3O_4 loading procedure was as follows: 1.6 g of treated CL was added to a mixed salt solution (bath ratio of 1 : 50) containing 0.56 g of $FeCl_3$ and 0.48 g of $FeSO_4 \cdot 7H_2O$. The solution was heated to 70 °C at a rotational speed of 400 rpm, and 1 M NaOH was added to adjust the pH to >9. The sample was then matured for 2 h and washed until the filtrate was completely transparent. The resulting sample was dried at 45 °C for 12 h in air to obtain the Fe_3O_4/CL adsorbent. Fe_3O_4/CL-O and Fe_3O_4/CL-D differ in the pretreatment process of CL. The oxidation pretreatment of CL involved adding 5 g of untreated CL to 250 ml of 2% NaOH solution and boiling for 30 min. The fiber was then filtered and transferred to 18% NaOH solution (bath ratio of 1 : 30) and stirred at room temperature for 2 h. After filtration and washing, the activated CL was obtained by drying at 45 °C for 12 h. The activated CL was placed into a 12 g L^{-1} $NaIO_4$ solution (bath ratio of 1 : 30), and the reaction was stirred continuously at 50 °C for 2 h in the absence of light. After the oxidation reaction, 3 ml of glycerol was added to remove the unreacted $NaIO_4$. Finally, the fibers were filtered, washed, and dried at 45 °C to form the treated CL-O. The precursor of Fe_3O_4/CL-D was synthesized by using the deep eutectic solvent (DES) dissolution method: 55.84 g of choline chloride and 55.04 g of oxalic acid dihydrate were stirred in a beaker at 90 °C until the reagent turned into a fully clarified liquid. Then, 1.0 g of CL was added into the solution until dissolved, it was filtered with ethanol and deionized water three times, and dried at 45 °C for 12 h. Subsequently, the dried fibers were mixed with deionized water at a ratio of 0.05% and ultrasonicated for 20 min, filtered with deionized water, and dried at 45 °C for 12 h to obtain CL-D.

2.2 Adsorbent characterization

The true content of Fe on the adsorbents was measured using inductively coupled plasma spectrometry (ICP-MS: Agilent 7800, USA). To analyze the crystal phases of all adsorbents, a Smartlab 9 kW advance powder X-ray Cu Kα radiation diffractometer (Japan) was used to record the X-ray diffraction (XRD) patterns of the samples, with the voltage at 40 kV, current at 40 mA, and the range of scan angle (2θ) set as 5–90°. The morphology and microstructure of the adsorbents were studied using field

emission scanning electron microscopy (SEM) on a ZEISS Sigma 300 (Germany). The Fourier transform infrared spectra of all adsorbents were recorded by a Thermo Scientific Nicolet iS50 FT-IR spectrometer (USA) in the range of 4000–450 cm^{-1}. The X-ray photoelectron spectroscopy (XPS) measurements of all adsorbents were carried out on a Thermo Scientific K-Alpha spectrometer (UK) equipped with a monochromatic Al K radiation source (1486.6 eV), and the values of binding energies were calibrated using the criterion reference of the C 1s signal at 284.8 eV. The thermogravimetric (TG) analysis of all adsorbents was carried out under a nitrogen atmosphere at a heating rate of 10 °C min^{-1} using a TA TGA5500 (USA).

2.3 Adsorption experiments

A series of adsorption experiments was conducted using the as-prepared adsorbents. In each experiment, 0.2 g of adsorbent was added to a 50 ml solution containing 1.0 g L^{-1} Cu^{2+} and stirred for 120 min using a magnetic agitator with varying speeds ranging from 200 to 600 rpm. The concentrations of remaining metal ions in the filtrate were determined using an atomic adsorption spectrophotometer (TAS-986, Beijing Purkinje General Instrument Co., Ltd). The adsorption capacity of the adsorbent was calculated as the difference between the initial and remaining concentrations of Cu^{2+}. The equilibrium adsorption capacity (eqn (1)) and the percentage removal of heavy metal ions (eqn (2)) were calculated using the following formulas:[44]

$$q_e = \frac{(C_0 - C_e)V}{m} \quad (1)$$

$$\text{Removal rate } (\%) = \frac{(C_0 - C_e)}{C_0} \times 100\% \quad (2)$$

Here, C_0 and C_e are the initial and equilibrium metal ion concentrations of Cu^{2+} (mg L^{-1}), respectively; V is the volume of the solutions used (L), and m is the amount (g) of adsorbent. To investigate the effect of temperature, stirring rate, and initial pH value on the adsorption capacity of the adsorbents, a series of adsorption experiments was conducted using a fixed concentration of Cu^{2+} at various temperatures in the range of 20–60 °C, stirring rate in the range of 200–600 rpm, and pH values ranging from 2.0 to 7.0. The adsorption isotherms were recorded by conducting adsorption experiments using different initial concentrations of Cu^{2+} ranging from 50 to 1000 mg g^{-1}. The adsorption kinetics were investigated by conducting adsorption experiments for different time intervals ranging from 1 to 420 min. To assess the regenerability of the adsorbent, a series of regeneration experiments was conducted using 0.1 M HCl as the regenerant, and the regenerated adsorbent was tested for its adsorption capacity towards Cu^{2+} in a new batch of solutions.

3 Results and discussion

3.1 Characterization of adsorbents

The actual Fe loadings recorded by ICP were 0, 0.19, 8.1, and 15.2 wt% for the CL, Fe_3O_4/CL, Fe_3O_4/CL-O, and Fe_3O_4/CL-D adsorbents, respectively. The results suggested that compared with untreated CL, the treated CL achieved higher Fe loadings, and the DES modified CL presented the maximum Fe loading. The XRD patterns of the adsorbents are shown in Fig. 2. The cotton linter (CL) exhibited obvious diffraction peaks at 14.9°, 16.5°, 22.7°, and 34.4°, which indicated that the natural cotton fibers used in the experiment had the typical cellulose type I crystal structure.[45] The characteristic peaks of Fe_3O_4/CL were mostly coincident with CL, which was due to the low loading of Fe_3O_4 on untreated CL and the limitations of XRD. Interestingly, only the characteristic peaks of cellulose could be observed for Fe_3O_4/CL-O, which may have been related to the high dispersion of Fe_3O_4 on the surface of CL-O, and this phenomenon was confirmed by SEM (Fig. 3). In addition to the presence of the obvious cellulose type I crystal characteristic peaks, diffraction peaks at 30.1°, 35.5°, 43.1°, 53.5°, 57.0°, and 62.7° were observed for Fe_3O_4/CL-D, which matched well with the pure magnetite reflections of Fe_3O_4 (PDF: 19-0629).[46] Moreover, the diffraction peak intensity of Fe_3O_4/CL-O and Fe_3O_4/CL-D decreased when modified by $NaIO_4$ oxidation or DES dissolution. At the same time, the macroscopic length and strength of the prepared Fe_3O_4/CL-O and Fe_3O_4/CL-D fibers became shorter and weaker, which indicated that the chemical

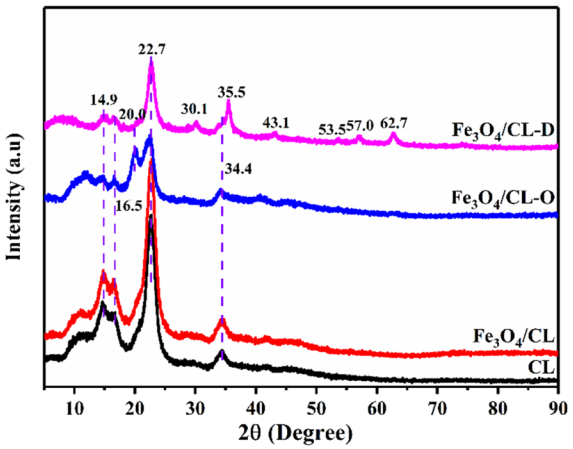

Fig. 2 XRD patterns of the adsorbents.

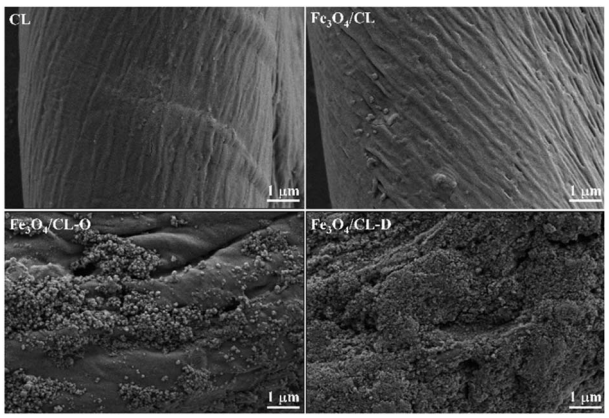

Fig. 3 SEM images of the adsorbents.

modification destroyed the internal structure of the cotton fibers. In other words, the crystallinity of Fe_3O_4/CL-O and Fe_3O_4/CL-D decreased and the fiber microstructure became looser, which we speculated was conducive to the diffusion of heavy metals into the fibers and favorable for adsorption.

Fig. 3 shows the SEM images of CL before and after modification. It can be observed that chemical modification changed the surface morphology of CL. Among them, the surface of CL appeared relatively smooth, while a few particles appeared on the surface of Fe_3O_4/CL. We speculated that these particles were Fe_3O_4 loaded on the surface of the fibers, and this phenomenon was more obvious on Fe_3O_4/CL-O and Fe_3O_4/CL-D. It is worth mentioning that this phenomenon was consistent with the increase of Fe loading in the ICP results. Besides, there were many grooves and folds on the surface of Fe_3O_4/CL-O, which was due to the oxidation and hydrolysis reaction between $NaIO_4$ and cellulose macromolecular chains on the surface of the cotton fibers, leading to the possible breakage of some cellulose molecular chains and the roughness of the fiber surface.[47] However, the surface of Fe_3O_4/CL-D was covered with so much Fe_3O_4 that it was difficult to distinguish, and the Fe_3O_4 underwent a certain extent of aggregation. It can be seen from the SEM images that the surface morphology of CL changed during chemical modification, and the surface changes of CL were most obvious due to the oxidation by $NaIO_4$ and the dissolution by the DES.

The crystalline structure of the adsorbents was analyzed using FTIR spectroscopy measurement, and the results are shown in Fig. 4. In the FTIR spectra, all samples presented six or more peaks corresponding to the typical cellulose crystal structure, which agreed with the XRD results. The peaks at 3420 cm^{-1}, 2900 cm^{-1}, 1640 cm^{-1}, 1427 cm^{-1}, 1060 cm^{-1}, and 896 cm^{-1} corresponded to O–H stretch vibrations, C–H stretch sp^3 vibrations, adsorbed water H_2O bending vibrations, C–H bending vibrations, C–O symmetric stretch vibrations, and glucoside bond vibrations, respectively.[48,49] These peaks are the characteristic adsorption peaks of cellulose, indicating that the main composition structure of cotton fiber did not change significantly after chemical modification. However, clear blue shifts for Fe_3O_4/CL-O and Fe_3O_4/CL-D were observed after chemical modification, such as the C–H stretch sp^3 vibration peak shift from 2921 cm^{-1} to 2895 cm^{-1}, and the glucoside bond shift from 899 cm^{-1} to 896 cm^{-1}, which indicated that the crystalline structure of CL slightly changed after $NaIO_4$ oxidation, DES dissolution, and Fe_3O_4 loading.[50,51]

The chemical valence states of each element in all adsorbents were further studied using X-ray photoelectron spectroscopy (XPS). In the broad spectrum (Fig. 5a), it was found that all the samples showed characteristic peaks belonging to C 1s and

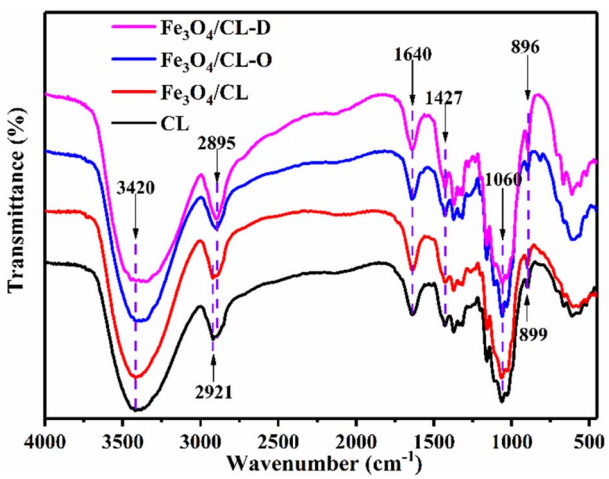

Fig. 4 FTIR spectra of the adsorbents.

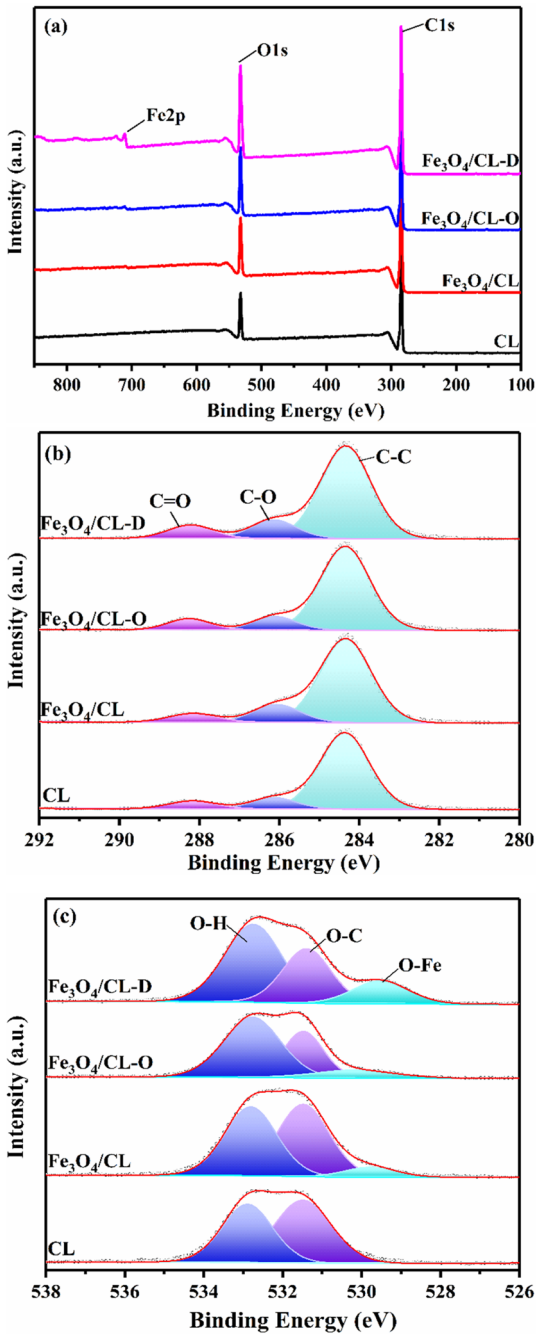

Fig. 5 XPS spectra of the adsorbents: (a) broad spectrum; (b) C 1s and (c) O 1s regions.

Table 1 Surface atomic content of the samples

Sample code	C atomic content	Fe atomic content	O atomic content
CL	84.46%	—	15.54%
Fe_3O_4/CL	83.40%	0.61%	15.99%
Fe_3O_4/CL-O	80.43%	0.98%	18.59%
Fe_3O_4/CL-D	75.76%	2.09%	22.15%

O 1s at 284.8 eV and 532.0 eV, indicating that there were carbon and oxygen elements in all the adsorbents and the content of carbon was higher than that of oxygen. Regarding the Fe 2p characteristic peak with binding energy near 711.0 eV, it was observed for Fe_3O_4/CL, Fe_3O_4/CL-O, and Fe_3O_4/CL-D, and it was most obvious for Fe_3O_4/CL-D, implying that the content of Fe element was the highest in Fe_3O_4/CL-D, and this result was consistent with the ICP result.[52] Subsequently, the high-resolution electronic spectra of C 1s were deconvolved (Fig. 5b), and the results showed that the carbon element in all samples had three kinds of chemical bonds, namely, C–C, C–O, and C=O, and the corresponding binding energy was around 284.5 eV, 286.2 eV, and 288.2 eV.[53,54] It should be noted that the presence of C=O in all the samples was caused by the interference of CO_2 in the air during the measurement, which was confirmed by the absence of C=O vibration peaks in the FTIR characterization. For the deconvolved O element (Fig. 5c), it was found that except for CL, the other adsorbents exhibited three valence forms of O, namely Fe–O at 529.7 eV, O–C at 531.5 eV, and O–H at 532.8 eV, respectively.[55,56] This result further indicated that except for CL, the other adsorbents were loaded with Fe to varying degrees and the Fe was present in the form of Fe–O bonds. Combined with XRD analysis, it was speculated that Fe was loaded on the cotton fibers in the form of Fe_3O_4, which provided the material basis for improving adsorption of metal ions (Cu^{2+}). Moreover, the surface atomic content of the samples was analyzed (Table 1), and it was found that with the chemical modification of CL, the proportion of C atoms gradually decreased, and correspondingly the proportion of Fe and O atoms gradually increased. The increased O atom content could greatly improve the coordination capacity of the samples, which would help to improve the adsorption capacity of the adsorbent for pollutants. Besides, it should be noted that the content of Fe atoms was significantly lower than that of the ICP results due to XPS being a surface-based technique.

The TG analysis of the samples is illustrated in Fig. 6. The TG curves show that two weight-loss processes occur in all the samples. The first weight loss stage occurred in the temperature range of 30–200 °C, which could be attributed to residual water evaporation.[57] The weight loss ratio of all samples at this stage was about 7%. When the temperature was higher than 200 °C, the main weight loss process occurred at 200–400 °C for all adsorbents, which resulted from the decomposition of the cotton fibers.[58] It should be noted that the weight loss amount for all samples was different; CL without any treatment underwent the highest weight loss (up to ~69%, water-loss part below 200 °C is not included in the calculation), followed by Fe_3O_4/CL

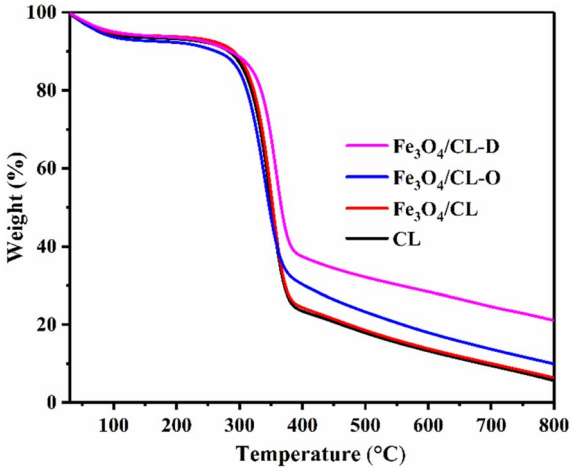

Fig. 6 TG curves of the adsorbents.

at ~67% and Fe_3O_4/CL-O at ~59%, and the lowest weight loss rate of ~52% for Fe_3O_4/CL-D. Therefore, it was speculated that the reason for the lower weight loss amounts of the other samples compared with CL was the successful loading of Fe_3O_4. ICP results showed that the content of Fe in Fe_3O_4 CL-D was the highest, followed by Fe_3O_4/CL-O and Fe_3O_4/CL, which further confirmed this phenomenon. The TG results suggested that the CL samples treated by $NaIO_4$ oxidation and DES dissolution were more likely to be loaded with Fe_3O_4, which had a positive influence on the adsorption of Cu^{2+}.

3.2 Evaluation of adsorbents

3.2.1 Adsorption properties of adsorbents. Before studying the adsorption properties of the adsorbents, the adsorption conditions were investigated and the results are illustrated in Fig. 7. It was observed that the removal efficiency was significantly influenced by the temperature, stirring rate, and initial

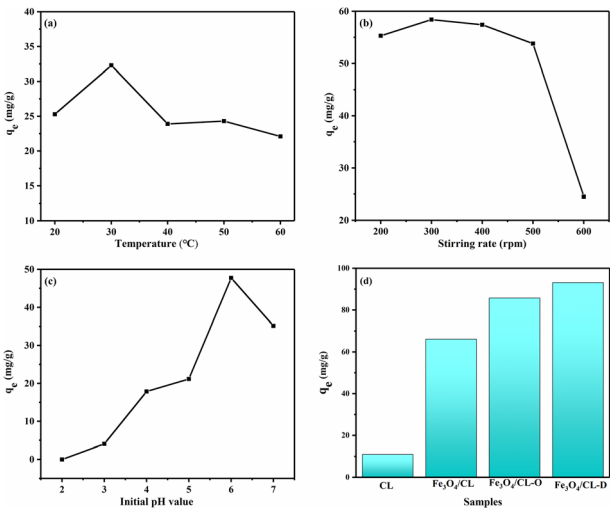

Fig. 7 Effect of temperature (a), stirring rate (b), and initial pH value (c) on the removal of Cu^{2+}; the adsorption capacity of all samples (d).

pH value. As the temperature increased to 30 °C, the adsorption capacity increased, but further increases in temperature led to a gradual decrease in adsorption capacity, possibly due to the increase in desorption capacity (Fig. 7a). Hence, 30 °C was selected as the adsorption temperature condition as it was close to room temperature and conducive to the further utilization of the adsorbent. The data on the influence of stirring speed indicated that the adsorption value remained relatively unchanged at rates between 200 and 500 rpm, but 300 rpm was found to be slightly advantageous (Fig. 7b). The effect of pH value on adsorption capacity was more pronounced, with the adsorption capacity increasing significantly with an increase in pH and reaching a maximum at around pH 6 (Fig. 7c). This was due to the deprotonation of the adsorbents, which increased with the pH value and enhanced the electrostatic attraction between the adsorbents and cations (Cu^{2+}), leading to an increase in adsorption capacity.[47] However, with a further increase in pH to 7, the adsorption capacity started to decrease due to protonation and the precipitation of some metal ions in a neutral environment.[46] Moreover, at alkaline pH, Cu ions reacted directly to form hydroxide precipitation, which was affected by the solubility product constant of $Cu(OH)_2$ and could compromise the accuracy of the adsorption experiment results.[59] As a result, further adsorption experiments were conducted with an initial pH value of 6.0, stirring rate of 300 rpm, and a temperature of 30 °C.

The adsorption capacity of all samples is presented in Fig. 7d. It was observed that CL showed a low adsorption activity of 11.0 mg g^{-1} before chemical modification and Fe_3O_4 loading. After the chemical modification and Fe_3O_4 loading treatment, the adsorption capacity of Fe_3O_4/CL, Fe_3O_4/CL-O, and Fe_3O_4/CL-D gradually increased and reached a maximum of 93.1 mg g^{-1} for Fe_3O_4/CL-D. These results indicated that Fe_3O_4 loading, $NaIO_4$ oxidation, and DES dissolution pretreatment positively contributed to further improving the adsorption property. We speculated that the increased adsorption capacity was due to the loading of Fe_3O_4, which increased the proportion of O atoms and improved the complexation ability of Cu ions. Moreover, $NaIO_4$ oxidation and DES dissolution caused significant damage to the structure of the cotton fibers, resulting in decreased fiber crystallinity and increased amorphous regions containing free hydroxyl groups, which was favorable for surface adsorption.

Furthermore, we compared the adsorption capacity of Fe_3O_4/CL-D with other biomaterials reported in previous studies and summarized the results in Table 2. One can find that the adsorption capacity of Fe_3O_4/CL-D for Cu^{2+} was higher than that of the reported related adsorbents. We believe that our Fe_3O_4/CL-D adsorbents have several advantages over other biomaterials. Firstly, our adsorbents have a high specific surface area due to the porous nature of cellulose, which provides more adsorption sites for heavy metal ions. Secondly, the use of Fe_3O_4 nanoparticles enhances the magnetic separation ability of the adsorbents, making them more efficient and cost-effective. Finally, the synthesis of the Fe_3O_4/CL-D adsorbents involves a simple and environmentally friendly method, which makes them suitable for large-scale production.

3.2.2 Adsorption behavior of adsorbents. To better explain the adsorption behavior, the Langmuir and Freundlich isothermal models were used to analyze the experimental data of Fe_3O_4/CL-D. The Langmuir adsorption isotherm model assumes that the surface of the adsorbent experiences monolayer adsorption, and there is no interaction between adsorbate molecules. This means that only molecules directly in contact with the surface of the adsorbent can be adsorbed, and the adsorbate can only form a layer on the surface of the adsorbent. The Langmuir model can be expressed by eqn (3):[46,60]

Langmuir model:

$$\frac{C_e}{Q_e} = \frac{C_e}{Q_{max}} + \frac{1}{K_L Q_{max}} \quad (3)$$

where Q_{max} is the Langmuir maximum adsorption capacity, Q_e is the equilibrium adsorption capacity, C_e is the adsorption equilibrium concentration, and K_L is the adsorption constant.

On the other hand, the Freundlich isotherm model assumes multilayer adsorption on a heterogeneous surface, and there are many interactions between adsorbent and adsorbate. Multilayer adsorption can be understood as the phenomenon whereby adsorbed molecules can re-adsorb with other molecules, meaning that indirect adsorption exists. The Freundlich isotherm model can be expressed by eqn (4):

Freundlich model:

$$\ln Q_e = \ln K_F + \frac{1}{n} \ln C_e \quad (4)$$

where K_F is the Freundlich adsorption coefficient, and n is the characteristic constant related to adsorption strength.

Table 2 Comparison of adsorption capacity of Fe_3O_4/CL-D for Cu^{2+} with previously reported adsorbents

Adsorbent	Cu^{2+} adsorption capacity (mg g^{-1})	Ref.
Fe_3O_4–cellulose–chitosan	44.7 ± 5	63
Magnetic chitosan/cellulose microspheres	88.21	64
p(HEMA-*co*-TACYC) hydrogels	17.24	65
Opuntia activated biochar (OFI)	49.36	66
SA-PAM/GO	68.76	67
Magnetic pine cone gel beads (MPCB)	69.80	60
Fe_3O_4/CL-D	93.1	This work

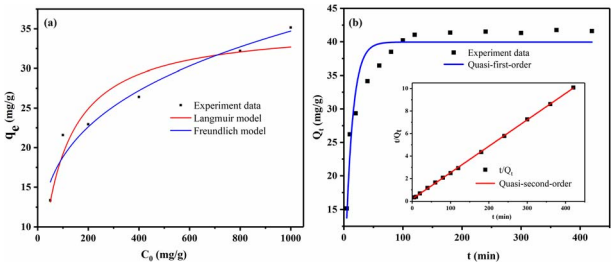

Fig. 8 The adsorption isotherms (a) and kinetics model (b) of Fe_3O_4/CL-D.

Table 3 Isotherm model parameters for Cu^{2+} adsorption using Fe_3O_4/CL-D

Langmuir			Freundlich		
$Q_{m,cal}$ (mg g^{-1})	K_L (L mg^{-1})	R^2	K_F	n	R^2
35.47	0.0118	0.9228	5.5259	4.2735	0.9540

Fig. 8a shows the fitting results of the Langmuir and Freundlich adsorption isotherm models to the experimental data, and the correlation coefficients of each model were calculated from the slope and intercept, as shown in Table 3. The models and parameter results indicated that, compared to the Langmuir isotherm model, the Freundlich isotherm model provided a better fit to the experimental data. This suggests that the adsorption of Cu^{2+} onto Fe_3O_4/CL-D is a multilayer process. We hypothesized that Cu^{2+} occupying the adsorption sites of Fe_3O_4 also undergoes hydrogen bonding or intermolecular adsorption with cotton fibers, facilitating continued indirect adsorption and leading to the diffusion of Cu ions into the interior of the adsorbent and the occurrence of multilayer adsorption.

The adsorption kinetics of a solute on an adsorbent is a fundamental parameter that determines the rate at which the reaction pollutant is adsorbed and the time required for the adsorbent to reach equilibrium. By controlling the residence time on the adsorbent at the solid–liquid interface, the efficiency of wastewater treatment can be improved. In this study, we investigated the adsorption kinetics of the adsorbent using both quasi-first-order and quasi-second-order kinetic models. The expressions for these models are given by eqn (5) and (6), respectively:[60]

Quasi-first-order kinetic model:

$$\ln(Q_e - Q_t) = \ln Q_t - k_1 t \quad (5)$$

Quasi-second-order kinetic model:

$$\frac{t}{Q_t} = \frac{t}{Q_e} + \frac{1}{k_2 Q_e^2} \quad (6)$$

where Q_e and Q_t are the amounts of pollutant adsorbed at equilibrium and at time t, respectively, k_1 is the rate constant of the quasi-first-order kinetic model, k_2 is the rate constant of the quasi-second-order kinetic model, and t is the contact time. These models can be used to accurately predict the adsorption behavior of the adsorbent and optimize the conditions for wastewater treatment.

Fig. 8b illustrates the adsorption kinetics curve of Cu^{2+} (experimental data), which shows that the adsorption equilibrium was reached after approximately 2 h. The adsorption process of Cu^{2+} was divided into three stages. The first stage was characterized by a rapid rise in the curve within the first 30 min of adsorption, indicating a high adsorption rate during this period, and adsorption mainly occurred on the surface of the adsorbent. In the second stage, the curve rose at a slower rate, and the adsorption capacity gradually stabilized between 30 and 120 min. The third stage, which occurred between 120 and 420 min, showed a stable adsorption capacity, indicating that the adsorption had reached equilibrium.[61] The initial rapid adsorption was attributed to the presence of numerous active adsorption sites or active groups on the surface of Fe_3O_4–CL-D that could combine with Cu^{2+}. As adsorption proceeded, the adsorption sites became progressively occupied, and competitive adsorption increased, resulting in a slower adsorption rate.

The fitted parameters of the adsorption kinetics curve of Cu^{2+} are listed in Table 4. Compared with the quasi-first-order kinetic model, the quasi-second-order kinetic model fits the experimental data better, with a fitting coefficient (R^2) close to 1.0, indicating that the quasi-second-order kinetic model can more reasonably describe the adsorption process of Cu^{2+} on Fe_3O_4–CL-D. The quasi-second-order kinetic model represents a second-order proportionality between the reaction rate and the square of the reactant concentration, reflecting the composite effect of adsorption and multiple adsorption mechanisms.

According to the presented information, Fe_3O_4–CL-D demonstrates a multilayer adsorption phenomenon for Cu^{2+} and conforms to both the Freundlich isothermal model and quasi-second-order adsorption mechanism. Specifically, Cu^{2+} adsorbed onto the surface of Fe_3O_4–CL-D to form a multilayer adsorption structure. This adsorption phenomenon can be accurately described by the Freundlich isothermal model, which indicates a power-law relationship between the adsorption capacity and the concentration of the adsorbate. Furthermore, this adsorption phenomenon follows the quasi-second-order adsorption mechanism, where the adsorption rate is proportional to the square of the concentration of the adsorbate. It is important to note that these findings have significant implications for understanding the adsorption behavior of Cu^{2+} on Fe_3O_4–CL-D and for developing new approaches for effective adsorption removal of heavy metals from contaminated water.

3.2.3 Dissociative and reabsorption behavior of adsorbents. In addition to the adsorption capacity of the CL-based

Table 4 Kinetic model parameters for Cu^{2+} adsorption using Fe_3O_4/CL-D

Pesudo-first-order			Pesudo-second-order		
Q_e (mg g^{-1})	k_1 (min^{-1})	R^2	Q_e (mg g^{-1})	k_2 (min^{-1})	R^2
39.9599	0.08435	0.9023	42.5894	0.00302	0.9997

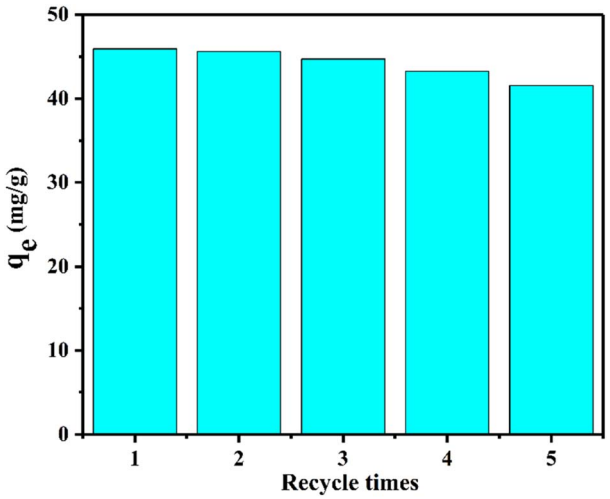

Fig. 9 Dissociative and reabsorption behavior of the adsorbent.

adsorbents, this study also investigated their regeneration capability to evaluate their sustainability and practical value. The results showed that the spent adsorbent particles could be desorbed and reused for multiple cycles, which could significantly reduce the cost of application and make them an environmentally friendly option. Specifically, Fe_3O_4/CL-D demonstrated excellent cycling performance, retaining about 97–98% of its initial adsorption capacity for Cu^{2+} after 4 cycles of adsorption (Fig. 9). This result indicates that the material has the potential to be a sustainable and efficient Cu^{2+} adsorbent in practical applications, emphasizing the importance of good cycling performance in evaluating the practical value of magnetic adsorbents. Overall, the study highlights the promising potential of the CL-based adsorbents as a sustainable and cost-effective option for water treatment.

3.3 Characterization of adsorbents after adsorption

To further elucidate the morphological and structural changes of the adsorbent after Cu^{2+} adsorption, Fourier-transform infrared (FTIR) spectroscopy and scanning electron microscopy (SEM) characterizations were performed on the corresponding samples, denoted by the suffix "U". Following the adsorption of Cu^{2+}, the material's functional groups and surface morphology underwent significant changes. The FTIR spectrum analysis revealed a weakening of peak intensities at 1427 cm^{-1}, 1060 cm^{-1}, and 896 cm^{-1}, corresponding to C–H, C–O, and glucoside bond vibrations after Cu^{2+} adsorption (Fig. 10).[49] This observation suggested that these functional groups played a significant role in the adsorption process. The overall FTIR peaks of all materials did not show any significant reduction, indicating that cellulose remained the primary constituent of the adsorbent.

Furthermore, the SEM images of the adsorbent before and after Cu^{2+} adsorption revealed changes in surface morphology (Fig. 11). Before adsorption, the surface of Fe_3O_4/CL was smooth and relatively uniform, whereas, after adsorption, the surface became porous and irregular with the formation of clusters. This suggested that the adsorption process led to the aggregation of adsorbent particles, which enhanced the adsorption capacity. The formation of these agglomerates may be attributed to the electrostatic attraction between the negatively charged surface of Fe_3O_4/CL-U and the positively charged Cu^{2+}. SEM analysis also revealed that the Fe_3O_4/CL-D-U sample retained its morphology and did not undergo significant structural changes after Cu^{2+} adsorption, indicating its stability and potential for reuse. These results provide further insights into the adsorption mechanism and structural properties of the Fe_3O_4/CL-D adsorbent, which can guide the design and optimization of similar adsorbents for efficient wastewater treatment applications.

3.4 Discussion of adsorption mechanism

A set of adsorbents comprising Fe_3O_4 on modified CL were synthesized using the coprecipitation method. Characterization using ICP, SEM, TG, and XRD revealed that Fe_3O_4 loading was maximal on Fe_3O_4/CL-D following DES dissolution, and crystallinity was correspondingly reduced to the greatest extent. Moreover, FTIR and XPS analyses demonstrated that the crystalline structure of CL underwent slight changes after chemical modification, with an increase in the proportion of O atoms that was favorable for Cu^{2+} adsorption. These findings contribute to our understanding of the adsorption behavior of Cu^{2+} on Fe_3O_4/CL-D and have important implications for the development of novel approaches for the effective removal of heavy metals from contaminated water sources.

The results presented in Fig. 7d demonstrate that the adsorption capacity of Cu^{2+} was significantly greater over Fe_3O_4/

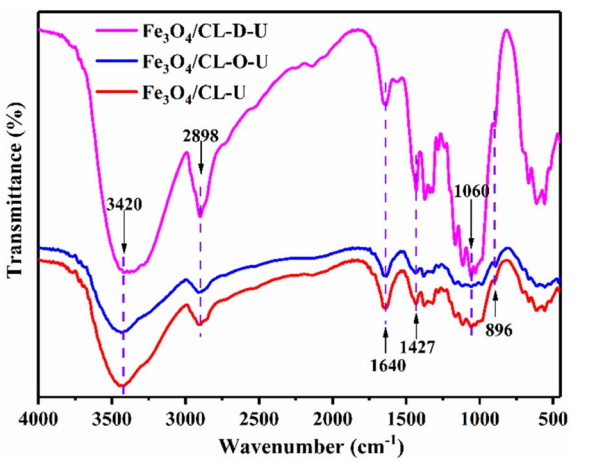

Fig. 10 FTIR spectra of the used adsorbents.

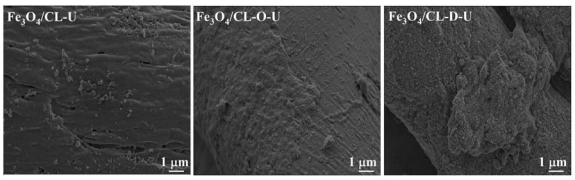

Fig. 11 SEM images of the used adsorbents.

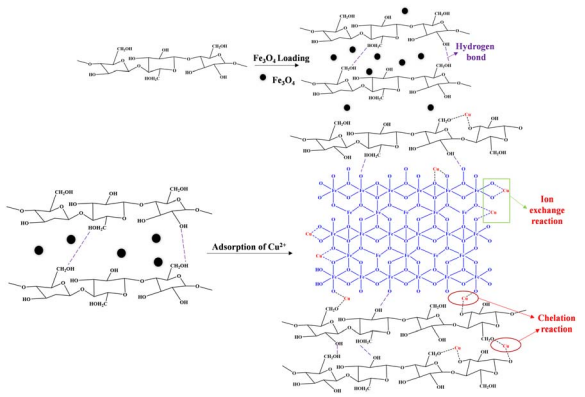

Fig. 12 The adsorption mechanism of Cu^{2+} by Fe_3O_4/CL-D in aqueous solution.

CL than CL. This enhanced performance can be attributed to the following factors: as indicated by the experimental results in Part 3.2.1 (Fig. 7c), the initial adsorption solution was weakly acidic, resulting in a large number of surface hydroxyl groups on the Fe_3O_4 molecule. These hydroxyl groups can interact with Cu^{2+} in the solution *via* ion exchange, leading to the efficient removal of Cu^{2+}. Furthermore, the pristine CL molecule possesses a multitude of hydroxyl groups, hydrogen bonds, and multilevel cavities, which facilitate chelation reactions with Cu^{2+}. However, the high crystallinity of CL hinders the entry of Cu^{2+} into the crystallization zone for coordination reactions, resulting in a very low adsorption rate for the unmodified CL. Therefore, oxidation by $NaIO_4$ and dissolution in DES were employed to decrease the crystallinity of cellulose and increase the accessibility of hydroxyl groups, resulting in an improved adsorption capacity of CL.

Through fitting the experimental data of the CL-based adsorbent using adsorption isotherm and kinetics models, we found that the adsorption of Cu^{2+} on Fe_3O_4/CL-D follows the Freundlich isotherm model and quasi-second-order adsorption model. Namely, the adsorption process of Cu^{2+} on Fe_3O_4/CL-D is multilayer and involves multiple adsorption mechanisms. Therefore, the adsorption mechanism of Cu^{2+} by Fe_3O_4/CL-D in aqueous solution was proposed as shown in Fig. 12.[62] Initially, Fe_3O_4 molecules were loaded onto the surface of CL, and the abundant O atoms in the molecular structure of Fe_3O_4 formed hydrogen bonds with the hydroxyl groups in CL molecules, thus stabilizing Fe_3O_4 on CL. Subsequently, the adsorption of Cu^{2+} on Fe_3O_4 was primarily driven by an ion exchange reaction, while the chelation reaction was mainly observed on the surface and interface of CL.

4 Conclusions

In this study, we successfully synthesized a magnetic Fe_3O_4/CL adsorption material using low-value cotton linter as the raw material. The chemical modification pretreatment of CL facilitated the loading of a higher amount of Fe_3O_4, particularly with the use of DES treatment, which effectively improved the adsorption capacity of Cu^{2+}. ICP analysis indicated that the Fe loading on Fe_3O_4/CL-D reached 15.2 wt% and existed in the form of Fe_3O_4, which was confirmed by XRD. Moreover, the XRD results suggested that the crystallinity of cotton linter treated with DES was significantly decreased, contributing to the increased accessibility of Cu^{2+} to hydroxyl groups and thus improving the adsorption capacity. As a result, the adsorption capacity of Fe_3O_4/CL-D reached 93.1 mg g^{-1}, which was much higher than that of untreated CL (11.0 mg g^{-1}). The adsorption process of Cu^{2+} on Fe_3O_4/CL-D from aqueous solution was an ion exchange and chelation reaction, and the adsorption behavior mainly involved Freundlich multimolecular layer adsorption and quasi-second-order multiple adsorption mechanisms. Our findings offer a potential strategy for the efficient utilization of low-cost cotton linter in the future, with broad application prospects in the adsorption of heavy metals and other pollutants. However, the current study also has limitations. For instance, the study only focused on the adsorption of Cu^{2+}, and the effectiveness of Fe_3O_4/CL-D for the adsorption of other pollutants was not investigated. In future research, the application of Fe_3O_4/CL-D in the removal of other heavy metals and pollutants will be explored. Additionally, the study only examined the feasibility of using cotton linter as a raw material for the synthesis of Fe_3O_4/CL-D. The scalability and economic feasibility of the production process should also be considered for practical applications.

Author contributions

S. Y.: conceptualization, formal analysis, resources; M. X.: formal analysis, investigation, writing – original draft; H. S.: methodology, formal analysis, writing – original draft; Y. N.: formal analysis, investigation, writing – review and editing; R. W.: resources, formal analysis; R. Y.: methodology, writing – review and editing; L. W.: methodology, validation; F. L.: project administration, funding acquisition, writing – review and editing; X. D.: visualization, funding acquisition, writing – review and editing; J. W.: conceptualization, formal analysis, writing – review and editing, supervision. All authors have read and agreed to the published version of the manuscript.

Conflicts of interest

There are no conflicts to declare.

Acknowledgements

The authors gratefully acknowledge the financial support from Young Talents Program of Anhui Academy of Agricultural Sciences, the Key Science and Technology Project of Anhui 334 Province (202003B06020009), Anhui Provincial Finance Agricultural Scientific and Technological Achievements Transformation Project (2022ZH011), and the Research Team Project of Anhui Academy of Agricultural Sciences.

References

1 J. Zhang, Z. Liu, B. Tian, J. Li, J. Luo, X. Wang, S. Ai and X. Wang, Assessment of soil heavy metal pollution in

provinces of China based on different soil types: From normalization to soil quality criteria and ecological risk assessment, *J. Hazard. Mater.*, 2023, **441**, 129891.

2 R. S. Ahmed, M. E. Abuarab, M. M. Ibrahim, M. Baioumy and A. Mokhtar, Assessment of environmental and toxicity impacts and potential health hazards of heavy metals pollution of agricultural drainage adjacent to industrial zones in Egypt, *Chemosphere*, 2023, 137872.

3 H. Binner, T. Sullivan, M. A. K. Jansen and M. E. McNamara, Metals in urban soils of Europe: A systematic review, *Sci. Total Environ.*, 2022, 158734.

4 J. d. S. O. Filho and M. G. Pereira, Is Environmental Contamination a Concern in Global Technosols? A Bibliometric Analysis, *Water, Air, Soil Pollut.*, 2023, **234**(3), 142.

5 Z. Wang, P. Luo, X. Zha, C. Xu, S. Kang, M. Zhou, D. Nover and Y. Wang, Overview assessment of risk evaluation and treatment technologies for heavy metal pollution of water and soil, *J. Cleaner Prod.*, 2022, 134043.

6 M. Wang, A. B. G. Janssen, J. Bazin, M. Strokal, L. Ma and C. Kroeze, Accounting for interactions between Sustainable Development Goals is essential for water pollution control in China, *Nat. Commun.*, 2022, **13**(1), 730.

7 Y. Yu, Y. Zhong, M. Wang and Z. Guo, Electrochemical behavior of aluminium anode in super-gravity field and its application in copper removal from wastewater by electrocoagulation, *Chemosphere*, 2021, **272**, 129614.

8 Y. Yu, Y. Zhong, W. Sun, J. Xie, M. Wang and Z. Guo, A novel electrocoagulation process with centrifugal electrodes for wastewater treatment: Electrochemical behavior of anode and kinetics of heavy metal removal, *Chemosphere*, 2023, **310**, 136862.

9 J. Gao, Y. Yuan, Q. Yu, B. Yan, Y. Qian, J. Wen, C. Ma, S. Jiang, X. Wang and N. Wang, Bio-inspired antibacterial cellulose paper-poly(amidoxime) composite hydrogel for highly efficient uranium(vi) capture from seawater, *Chem. Commun.*, 2020, **56**(28), 3935–3938.

10 V. Mohanapriya, R. Sakthivel, N. D. K. Pham, C. K. Cheng, H. S. Le and T. M. H. Dong, Nanotechnology - A ray of hope for heavy metals removal, *Chemosphere*, 2023, **311**, 136989.

11 S. Rajendran, A. K. Priya, P. S. Kumar, T. K. A. Hoang, K. Sekar, K. Y. Chong, K. S. Khoo, H. S. Ng and P. L. Show, A critical and recent developments on adsorption technique for removal of heavy metals from wastewater-A review, *Chemosphere*, 2022, **303**, 135146.

12 Z. Long, Q. Li, T. Wei, G. Zhang and Z. Ren, Historical development and prospects of photocatalysts for pollutant removal in water, *J. Hazard. Mater.*, 2020, **395**, 122599.

13 A. Guleria, R. Sharma, P. Shandilya, Photocatalytic and adsorptional removal of heavy metals from contaminated water using nanohybrids, *Materials and Research Foundations*, 2021, vol. 100, pp. 113–160.

14 A. E. Mouden, N. E. Messaoudi, A. E. Guerraf, A. Bouich, V. Mehmeti, A. Lacherai, A. Jada and F. Sher, Multifunctional cobalt oxide nanocomposites for efficient removal of heavy metals from aqueous solutions, *Chemosphere*, 2023, 137922.

15 G. Lin, B. Zeng, J. Li, Z. Wang, S. Wang, T. Hu and L. Zhang, A systematic review of metal organic frameworks materials for heavy metal removal: synthesis, applications and mechanism, *Chem. Eng. J.*, 2023, **460**, 141710.

16 D. Li, X. Tian, Z. Wang, Z. Guan, X. Li, H. Qiao, H. Ke, L. Luo and Q. Wei, Multifunctional adsorbent based on metal-organic framework modified bacterial cellulose/chitosan composite aerogel for high efficient removal of heavy metal ion and organic pollutant, *Chem. Eng. J.*, 2020, **383**, 123127.

17 R. Liu, S. Wen, Y. Sun, B. Yan, J. Wang, L. Chen, S. Peng, C. Ma, X. Cao, C. Ma, G. Duan, S. Shi, Y. Yuan and N. Wang, A nanoclay enhanced Amidoxime-Functionalized Double-Network hydrogel for fast and massive uranium recovery from seawater, *Chem. Eng. J.*, 2021, **422**, 130060.

18 J. Yu, A. C. Wang, M. Zhang and Z. Lin, Water treatment *via* non-membrane inorganic nanoparticles/cellulose composites, *Mater. Today*, 2021, **50**, 329–357.

19 A. K. Rana, S. Guleria, V. K. Gupta and V. K. Thakur, Cellulosic pine needles-based biorefinery for a circular bioeconomy, *Bioresour. Technol.*, 2023, **367**, 128255.

20 A. K. Rana, F. Scarpa and V. K. Thakur, Cellulose/polyaniline hybrid nanocomposites: Design, fabrication, and emerging multidimensional applications, *Ind. Crops Prod.*, 2022, **187**, 115356.

21 A. K. Badawi, M. Abd Elkodous and G. A. M. Ali, Recent advances in dye and metal ion removal using efficient adsorbents and novel nano-based materials: an overview, *RSC Adv.*, 2021, **11**(58), 36528–36553.

22 A. Sczostak, Cotton Linters: An Alternative Cellulosic Raw Material, *Macromol. Symp.*, 2010, **294**(2), 151.

23 J. P. Morais, F. Rosa Mde, S. de Souza Filho Mde, L. D. Nascimento, D. M. do Nascimento and A. R. Cassales, Extraction and characterization of nanocellulose structures from raw cotton linter, *Carbohydr. Polym.*, 2013, **91**(1), 229–235.

24 X. Zhou, P. Wang, Y. Zhang, X. Zhang and Y. Jiang, From Waste Cotton Linter: A Renewable Environment-Friendly Biomass Based Carbon Fibers Preparation, *ACS Sustainable Chem. Eng.*, 2016, **4**(10), 5585–5593.

25 A. Tutuş, A. Özdemir and M. Çiçekler, Evaluation of Linter Cellulose as an Alternative Raw Material for Tissue Paper Production, *Drvna Ind.*, 2017, **68**(4), 291–298.

26 Y. Sun, Q. Yue, B. Gao, Q. Li, L. Huang, F. Yao and X. Xu, Preparation of activated carbon derived from cotton linter fibers by fused NaOH activation and its application for oxytetracycline (OTC) adsorption, *J. Colloid Interface Sci.*, 2012, **368**(1), 521–527.

27 A. Etale, A. J. Onyianta, S. R. Turner and S. J. Eichhorn, Cellulose: A Review of Water Interactions, Applications in Composites, and Water Treatment, *Chem. Rev.*, 2023, **123**(5), 2016–2048.

28 T. Li, C. Chen, A. H. Brozena, J. Y. Zhu, L. Xu, C. Driemeier, J. Dai, O. J. Rojas, A. Isogai, L. Wagberg and L. Hu, Developing fibrillated cellulose as a sustainable technological material, *Nature*, 2021, **590**(7844), 47–56.

29 H. Wang, G. Gurau and R. D. Rogers, Ionic liquid processing of cellulose, *Chem. Soc. Rev.*, 2012, **41**(4), 1519–1537.
30 O. M. Vanderfleet and E. D. Cranston, Production routes to tailor the performance of cellulose nanocrystals, *Nat. Rev. Mater.*, 2020, **6**(2), 124–144.
31 Z. Ling, J. V. Edwards, Z. Guo, N. T. Prevost, S. Nam, Q. Wu, A. D. French and F. Xu, Structural variations of cotton cellulose nanocrystals from deep eutectic solvent treatment: micro and nano scale, *Cellulose*, 2018, **26**(2), 861–876.
32 Z. Ling, T. Wang, M. Makarem, M. Santiago Cintrón, H. N. Cheng, X. Kang, M. Bacher, A. Potthast, T. Rosenau, H. King, C. D. Delhom, S. Nam, J. Vincent Edwards, S. H. Kim, F. Xu and A. D. French, Effects of ball milling on the structure of cotton cellulose, *Cellulose*, 2019, **26**(1), 305–328.
33 L. Zhou, F. Pan, Y. Liu, Z. Kang, S. Zeng and Y. Nie, Study on the regularity of cellulose degradation in ionic liquids, *J. Mol. Liq.*, 2020, **308**, 113153.
34 A. J. Sayyed, N. A. Deshmukh and D. V. Pinjari, A critical review of manufacturing processes used in regenerated cellulosic fibres: viscose, cellulose acetate, cuprammonium, LiCl/DMAc, ionic liquids, and NMMO based lyocell, *Cellulose*, 2019, **26**(5), 2913–2940.
35 R. Sescousse, R. Gavillon and T. Budtova, Aerocellulose from cellulose–ionic liquid solutions: Preparation, properties and comparison with cellulose–NaOH and cellulose–NMMO routes, *Carbohydr. Polym.*, 2011, **83**(4), 1766–1774.
36 R. P. Swatloski, J. D. Holbrey and R. D. Rogers, Ionic liquids are not always green: hydrolysis of 1-butyl-3-methylimidazolium hexafluorophosphate, *Green Chem.*, 2003, **5**, 361–363.
37 R. P. Swatloski, S. K. Spear, J. D. Holbrey and R. D. Rogers, Dissolution of Cellose with Ionic Liqui, *J. Am. Chem. Soc.*, 2002, **124**(18), 4974–4975.
38 R. D. Rogers and K. R. Seddon, CHEMISTRY: Ionic Liquids–Solvents of the Future?, *Science*, 2003, **302**(5646), 792–793.
39 A. Mnasri, R. Khiari, H. Dhaouadi, S. Halila and E. Mauret, Acidic and alkaline deep eutectic solvents pre-treatment to produce high aspect ratio microfibrillated cellulose, *Bioresour. Technol.*, 2023, **368**, 128312.
40 J. Xie, J. Xu, Z. Zhang, B. Wang, S. Zhu, J. Li and K. Chen, New ternary deep eutectic solvents with cycle performance for efficient pretreated radiata pine forming to lignin containing cellulose nanofibrils, *Chem. Eng. J.*, 2023, **451**, 138591.
41 X. Wu, Y. Yuan, S. Hong, J. Xiao, X. Li and H. Lian, Controllable preparation of nano-cellulose *via* natural deep eutectic solvents prepared with lactate and choline chloride, *Ind. Crops Prod.*, 2023, **194**, 116259.
42 M. P. Rayaroth, D. Oh, C.-S. Lee and Y.-S. Chang, Simultaneous removal of heavy metals and dyes in water using a MgO-coated Fe_3O_4 nanocomposite: Role of micro-mixing effect induced by bubble generation, *Chemosphere*, 2022, **294**, 133788.
43 E. S. Behbahani, K. Dashtian and M. Ghaedi, Fe_3O_4-$FeMoS_4$: Promise magnetite LDH-based adsorbent for simultaneous removal of Pb (II), Cd (II), and Cu (II) heavy metal ions, *J. Hazard. Mater.*, 2021, **100**.
44 M. E. Mahmoud, S. M. El-Bahy and S. M. T. Elweshahy, Decorated Mn-ferrite nanoparticle@Zn-Al layered double hydroxide@Cellulose@ activated biochar nanocomposite for efficient remediation of methylene blue and mercury (II), *Bioresour. Technol.*, 2021, **342**, 126029.
45 X. Deng, S. Ye, L. Wan, J. Wu, H. Sun, Y. Ni and F. Liu, Study on Dissolution and Modification of Cotton Fiber in Different Growth Stages, *Materials*, 2022, **15**(7), 2685.
46 H. L. Fan, S. F. Zhou, W. Z. Jiao, G. S. Qi and Y. Z. Liu, Removal of heavy metal ions by magnetic chitosan nanoparticles prepared continuously *via* high-gravity reactive precipitation method, *Carbohydr. Polym.*, 2017, **174**, 1192–1200.
47 X. Yue, F. Jiang, D. Zhang, H. Lin and Y. Chen, Preparation of adsorbent based on cotton fiber for removal of dyes, *Fibers Polym.*, 2017, **18**(11), 2102–2110.
48 Y. Yue, G. Han and Q. Wu, Transitional Properties of Cotton Fibers from Cellulose I to Cellulose II Structure, *BioResources*, 2013, **8**(4), 6460–6471.
49 T. Chen, J. Hong, C. Peng, G. Chen, C. Yuan, Y. Xu, B. Zeng and L. Dai, Superhydrophobic and flame retardant cotton modified with DOPO and fluorine-silicon-containing crosslinked polymer, *Carbohydr. Polym.*, 2019, **208**, 14–21.
50 N. Abidi, L. Cabrales and C. H. Haigler, Changes in the cell wall and cellulose content of developing cotton fibers investigated by FTIR spectroscopy, *Carbohydr. Polym.*, 2014, **100**, 9–16.
51 M. Martinez-Sanz, F. Pettolino, B. Flanagan, M. J. Gidley and E. P. Gilbert, Structure of cellulose microfibrils in mature cotton fibres, *Carbohydr. Polym.*, 2017, **175**, 450–463.
52 T. Yamashita and P. Hayes, Analysis of XPS spectra of Fe^{2+} and Fe^{3+} ions in oxide materials, *Appl. Surf. Sci.*, 2008, **254**(8), 2441–2449.
53 X. Chen, X. Wang and D. Fang, A review on C1s XPS-spectra for some kinds of carbon materials, *Fullerenes, Nanotubes, Carbon Nanostruct.*, 2020, **28**(12), 1048–1058.
54 M. Ayiania, M. Smith, A. J. R. Hensley, L. Scudiero, J.-S. McEwen and M. Garcia-Perez, Deconvoluting the XPS spectra for nitrogen-doped chars: An analysis from first principles, *Carbon*, 2020, **162**, 528–544.
55 Q. Li, H. Wang, Z. Chen, X. He, Y. Liu, M. Qiu and X. Wang, Adsorption-reduction strategy of U(VI) on NZVI-supported zeolite composites *via* batch, visual and XPS techniques, *J. Mol. Liq.*, 2021, **339**, 116719.
56 P. S. Bagus, C. J. Nelin, C. R. Brundle, N. Lahiri, E. S. Ilton and K. M. Rosso, Analysis of the Fe 2p XPS for hematite alpha Fe_2O_3: Consequences of covalent bonding and orbital splittings on multiplet splittings, *J. Chem. Phys.*, 2020, **152**(1), 014704.
57 G. Zhu, L. Yang, Y. Gao, J. Xu, H. Chen, Y. Zhu, Y. Wang, C. Liao, C. Lu and C. Zhu, Characterization and pelletization of cotton stalk hydrochar from HTC and combustion kinetics of hydrochar pellets by TGA, *Fuel*, 2019, **244**, 479–491.

58 M. Zhong, S. Chen, T. Wang, J. Liu, M. Mei and J. Li, Co-pyrolysis of polyester and cotton *via* thermogravimetric analysis and adsorption mechanism of Cr (VI) removal by carbon in aqueous solution, *J. Mol. Liq.*, 2022, **354**, 118902.

59 M. S. Almughamisi, Z. A. Khan, W. Alshitari and K. Z. Elwakeel, Recovery of Chromium(VI) Oxyanions from Aqueous Solution Using $Cu(OH)_2$ and CuO Embedded Chitosan Adsorbents, *J. Polym. Environ.*, 2019, **28**(1), 47–60.

60 M. Touihri, F. Guesmi, C. Hannachi, B. Hamrouni, L. Sellaoui, M. Badawi, J. Poch and N. Fiol, Single and simultaneous adsorption of Cr(VI) and Cu (II) on a novel Fe_3O_4/pine cones gel beads nanocomposite: Experiments, characterization and isotherms modeling, *Chem. Eng. J.*, 2021, **416**, 129101.

61 X. Yue, J. Huang, F. Jiang, H. Lin and Y. Chen, Synthesis and characterization of cellulose-based adsorbent for removal of anionic and cationic dyes, *J. Eng. Fibers Fabr.*, 2019, **14**, DOI: **10.1177/1558925019828194**.

62 S. Ye, H. Sun, J. Wu, L. Wan, Y. Ni, R. Wang, Z. Xiang and X. Deng, Supercritical CO_2 Assisted TiO_2 Preparation to Improve the UV Resistance Properties of Cotton Fiber, *Polymers*, 2022, **14**, 5513.

63 Z. Liu, H. Wang, C. Liu, Y. Jiang, G. Yu, X. Mu and X. Wang, Magnetic cellulose-chitosan hydrogels prepared from ionic liquids as reusable adsorbent for removal of heavy metal ions, *Chem. Commun.*, 2012, **48**(59), 7350–7352.

64 X. Luo, J. Zeng, S. Liu and L. Zhang, An effective and recyclable adsorbent for the removal of heavy metal ions from aqueous system: Magnetic chitosan/cellulose microspheres, *Bioresour. Technol.*, 2015, **194**, 403–406.

65 H. Ozay, Z. Gungor, B. Yilmaz, P. Ilgin and O. Ozay, Dual use of colorimetric sensor and selective copper removal from aqueous media with novel p(HEMA-*co*-TACYC) hydrogels: Cyclen derivative as both monomer and crosslinker, *J. Hazard. Mater.*, 2020, **389**, 121848.

66 M. Choudhary, R. Kumar and S. Neogi, Activated biochar derived from Opuntia ficus-indica for the efficient adsorption of malachite green dye, Cu(+2) and Ni(+2) from water, *J. Hazard. Mater.*, 2020, **392**, 122441.

67 H. Jiang, Y. Yang, Z. Lin, B. Zhao, J. Wang, J. Xie and A. Zhang, Preparation of a novel bio-adsorbent of sodium alginate grafted polyacrylamide/graphene oxide hydrogel for the adsorption of heavy metal ion, *Sci. Total Environ.*, 2020, **744**, 140653.